Journal for ImmunoTherapy of Cancer

Effects of oncolytic immunotherapy with RP1 (vusolimogene oderparepvec) on immune cells mediate responsiveness to anti-PD-1 via STING-mediated interferon signaling

Victoria Roulstone ,[1] Joan Kyula,[1] Elizabeth Appleton,[1] Praveen K Bommareddy,[2] Anton Patrikeev ,[1] Sylwia Jones,[2] Linta Kuncheria,[2] Charleen ML Chan Wah Hak ,[1] Shane Foo,[1] Holly Baldock,[1] Amarin Wongariyapak,[1] Isla Leslie,[1] Robert Pickering ,[1] Christian Zierhut ,[1] Henry G Smith,[1] Nitya Mohan,[1] Carmen Murano,[1] Lisa C Hubbard ,[1] Isaac Dean ,[1] Emmanuel Christian Patin ,[1] Jim Gkantalis ,[1] David Mansfield,[1] Malin Pedersen ,[1] Martin McLaughlin ,[1] Maria Goicoechea,[1] Scott Layzell,[1] Jonathan Mannion ,[1] Winnie Fernando,[1] Pascal Meier,[1] Richard Vile,[3] Alan Melcher ,[1] Robert S Coffin,[2] Kevin J Harrington [1]

To cite: Roulstone V, Kyula J, Appleton E, *et al*. Effects of oncolytic immunotherapy with RP1 (vusolimogene oderparepvec) on immune cells mediate responsiveness to anti-PD-1 via STING-mediated interferon signaling. *Journal for ImmunoTherapy of Cancer* 2026;**14**:e013692. doi:10.1136/jitc-2025-013692

► Additional supplemental material is published online only. To view, please visit the journal online (https://doi.org/10.1136/jitc-2025-013692).

VR, JK and EA contributed equally.

Accepted 07 February 2026

For numbered affiliations see end of article.

Correspondence to
Victoria Roulstone;
victoria.roulstone@icr.ac.uk

ABSTRACT

Background Antitumor immune responses induced by oncolytic immunotherapy (OI) are often followed by upregulation of programmed death-ligand 1 (PD-L1). As such, the combination of OI with blockade of the programmed cell death protein-1 (PD-1)/PD-L1 axis has demonstrated therapeutic activity in preclinical and clinical trials. The purpose of this study is to understand further the immune-mediated mechanism of interaction between oncolytic viruses and anti-PD-1 therapy.

Methods Tumor cells and immune cells (splenocytes) were cultured separately, or in co-culture with vusolimogene oderparepvec, an oncolytic herpes simplex virus expressing the fusogenic gibbon-ape leukemia virus-fusogenic membrane glycoprotein protein (GALV) and granulocyte-macrophage colony-stimulating factor (GM-CSF), also known as RP1. Viral replication, interferon (IFN) responses and PD-L1 expression were analyzed using wild-type, IFNAR1, TNFAR1 and STING knockout splenocytes. In vivo studies evaluated immune cell infiltrates into the tumor following RP1 administration with anti-PD-1 therapy.

Results RP1 replication was evident in tumor cells but not splenocytes. This was also accompanied by upregulated IFN expression in cultured splenocytes that was absent in cultured tumor cells. However, when these cell types were co-cultured, splenocytes mediated an interferon response to RP1 via STING that was transmitted to tumor cells in a non-touch-dependent manner. Tumor cells responded to these input signals via upregulation of cell surface major histocompatibility complex-I and PD-L1 through tumor intrinsic JAK-STAT signaling. In vivo, an IFN signature was observed following intratumoral injection of RP1, both in injected and non-injected tumors, which was further increased when combined with anti-PD-1 therapy. Marked upregulation of PD-L1 was observed in tumors injected with RP1 accompanied by the recruitment of CD11b+Ly6G+neutrophils into the tumor microenvironment, which stained positive for PD-L1.

Conclusion Overall, the data demonstrate that RP1 remodels the tumor microenvironment through a combination of direct and indirect effects on both tumor and immune cells, resulting in an overall more inflamed phenotype.

INTRODUCTION

Viruses with selective tropism for or selective cytotoxic properties against tumors have been the subject of intense research for a number of decades. Initially, oncolytic viruses were viewed in much the same way as conventional cytotoxic chemotherapy agents, in that their main mechanism of action was thought to be direct virus-mediated cancer cell killing. Over the last two decades, however, this view has shifted to a position in which they are largely viewed as a branch of anticancer immunotherapy,[1 2] and are hence often referred to as oncolytic immunotherapies (OIs). The herpes simplex virus (HSV)-based OI, talimogene laherparepvec (T-VEC), was US Food and Drug Administration (FDA) approved as a monotherapy for the treatment of melanoma in 2015[3] based on the pivotal OPTiM phase III study. However, a subsequent, randomized phase III study, MASTERKEY-265, of pembrolizumab with or without T-VEC in previously untreated patients with melanoma did not demonstrate superior

WHAT IS ALREADY KNOWN ON THIS TOPIC

⇒ Oncolytic virotherapy can induce antitumor immune responses and lead to an inflamed tumor microenvironment. In the IGNYTE clinical trial, vusolimogene oderparepvec, an oncolytic herpes simplex virus expressing the fusogenic gibbon-ape leukemia virus-fusogenic membrane glycoprotein (GALV) protein and granulocyte-macrophage colony-stimulating factor (GM-CSF), also known as RP1, was combined with anti-programmed cell death protein-1 (PD-1) therapy and led to a 33% response rate. However, it is incompletely understood how RP1 can influence immune cell populations, and how tumor and immune cells interact in the context of interferons (IFNs) and programmed death-ligand 1 (PD-L1) expression.

WHAT THIS STUDY ADDS

⇒ This study demonstrates distinct responses to RP1 between tumor and immune cells, and how tumor cells coordinate responses to the signals generated by immune cells. Our findings provide a mechanistic insight into how RP1 reshapes the tumor microenvironment and highlight the importance of STING in activating RP1-induced IFN responses in immune cells, which drive PD-L1 expression.

HOW THIS STUDY MIGHT AFFECT RESEARCH, PRACTICE OR POLICY

⇒ This study supports the rationale for combining RP1 with PD-1/PD-L1 checkpoint inhibition, and may help guide rational design of combination strategies with oncolytic viruses in order to maximize systemic antitumor immunity.

efficacy of the combination, and other studies have not demonstrated meaningful clinical benefit of T-VEC in patients post-progression on anti-programmed cell death protein-1 (PD-1) therapy.[4]

Intending to improve on both the direct tumor killing and systemic immune activation able to be achieved with T-VEC, a next-generation oncolytic HSV immunotherapy, vusolimogene oderparepvec (VO, also known as RP1), was developed. RP1 is based on a new clinical strain of HSV, intended to improve direct oncolytic destruction of tumors, and in addition to granulocyte-macrophage colony-stimulating factor (GM-CSF), encodes the gibbon-ape leukemia virus (GALV) fusogenic membrane glycoprotein (GALV-GP R-) to further improve direct tumor destruction, the immunogenicity of cell death, and systemic antitumor immune activation. In the IGNYTE clinical trial in anti-PD-1 failed melanoma in combination with nivolumab, a 33% response rate with strong durability was shown in 140 patients,[5] with similar responses in both injected and non-injected lesions, including visceral lesions. Analysis of biomarkers in a subset of patients with pretreatment and on-treatment biopsy samples demonstrated increases in immune cell infiltration, inflammatory gene expression and programmed death-ligand 1 (PD-L1) staining.[5]

With the objective of further understanding the detailed immune-mediated mechanism of action of RP1, we used immunocompetent murine models to further interrogate these immune effects, which also has the potential to inform the development of future combination strategies. Our studies show that RP1 (in these studies, a version expressing mouse rather than human GM-CSF was used) does not induce PD-L1 expression directly in murine tumor cells in vitro. Instead, lymphocytes sense RP1 via the STING pathway, with resulting interferon (IFN) signaling. In co-culture experiments in vitro, this increases PD-L1 expression in both immune and tumor cell compartments and, in the latter, major histocompatibility complex (MHC) class I expression is also increased. In vivo in mice, an IFN signature is observed following intratumoral injections of RP1 and this is amplified with anti-PD-1 therapy. Tumors injected with RP1 display marked upregulation of PD-L1, accompanied by the recruitment of large numbers of PD-L1-expressing CD11b+Ly6G+neutrophils into the tumor. These data add further depth to our understanding of RP1 as a potent, multifaceted OI and provide rationale for additional therapeutic combinations.

RESULTS

RP1 therapy results in an interferon response signature, which is boosted by anti-PD-1

To mirror the clinical setting where RP1 is given with PD-1 immune checkpoint inhibition, we used a version of RP1 which expresses murine rather than human GM-CSF, in immunocompetent C57BL/6 mice. The details of the isolation and genetic engineering of this virus are shown in (online supplemental figure S1A), and as previously described.[6] Briefly, the genetic variation between strains of HSV-1 was sampled by screening 29 new clinical strains isolated from volunteers who suffer from recurrent cold sores across a panel of human tumor cell lines to identify the strain to be developed. This strain (RH018A) was then engineered for use as an oncolytic virus by deletion of the genes encoding ICP34.5 to reduce pathogenicity, deleting the ICP47-encoding gene to enhance viral and tumor antigen presentation by MHC-I, and inserting a gene encoding a potent fusogenic glycoprotein derived from GALV-GP-R-. Expression of GALV-GP-R- caused increased immunogenic cell death. Initially, we sought to explore effects in non-injected lesions by treating animals with bi-flank tumors with multiple intratumoral doses of RP1 on only one side. While murine cells are generally far less susceptible to HSV than are human cells, the 4434 mouse $BRAF^{V600E}$ mutant melanoma cell line was chosen because it has a reasonable level of permissivity to HSV and therefore susceptibility to RP1 in vitro (online supplemental figure S1B), and it is a melanoma cell line, the tumor type for which RP1 is expected to be FDA approved. Therapeutic efficacy was observed in both injected lesions and in non-injected tumors to a lesser extent (figure 1A).

To map lymphatic drainage, Evans blue dye was injected intratumorally and distribution assessed (online supplemental figure S1C). The dye drained to both inguinal and axillary lymph nodes on the injected but

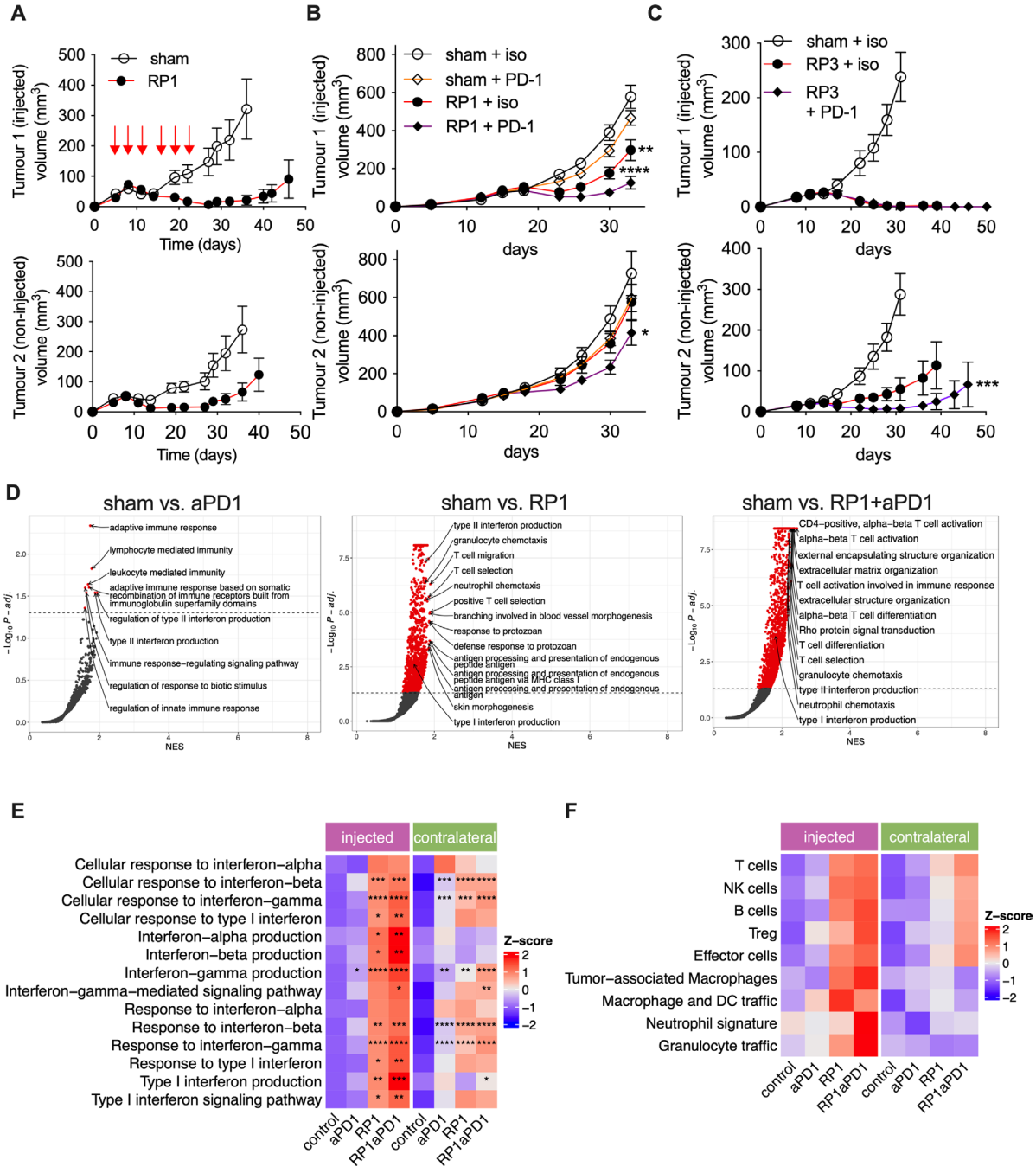

Figure 1 RP1 therapy is associated with an interferon response signature, which is boosted by anti-PD-1. (A) Tumor volumes for C57BL/6 mice bearing bi-flank 4434 tumors were injected in one flank with six doses of 5×10^6 pfu RP1 (n=11) or sham injection of formulation buffer (n=11). (B) Tumor volumes for C57BL/6 mice bearing bi-flank 4434 tumors were injected in one flank with three doses of 5×10^6 pfu RP1 (n=9), or sham injection of formulation buffer (n=12), three doses of anti-PD-1 at 10 mg/kg (BE0146, RMP1-14 CD279 invivoMAb) given I.P. (n=12), or the combination (concomitantly, n=12). P values were derived from one-way ANOVA adjusted for multiple comparisons, from area under curve values from individual mice. (C) Tumor volumes for C57BL/6 mice bearing bi-flank 4434 tumors were injected in one flank with three doses of 5×10^6 pfu of the murine version of RP3 (n=8), or sham injection of formulation buffer (n=6), or three doses of anti-PD-1 at 10 mg/kg given with RP3 (concomitantly, n=9). P values were derived from one-way ANOVA adjusted for multiple comparisons, from area under curve values from individual mice. (D) RNA-seq data from 4434 tumors treated as described in B, and collected day 8 after the first injection. Data show half-volcanoes for top 10 upregulated GO:BP, type 1/2 IFN production and neutrophils/granulocytes chemotaxis in injected tumors. Data represent n=5 tumors per group. (E) Heatmaps corresponding to IFN signature gene expression from RNA-seq data from 4434 tumors treated as described in B. Data represent n=5 tumors per group. (F) Cell type signatures heatmap. Immune cell scoring was performed on normalized RNA-seq counts from 4434 tumors treated as described in B, using the mMCP-counter package. Data represent n=5 tumors per group. P values were derived where p>0.05 ns, *p≤0.05, **p≤0.01, ***p≤0.001, ****p≤0.0001. ANOVA, analysis of variance; BP, Biological Processes; GO, Gene Ontology; IFN, interferon; I.P., intraperitoneal; PD-1, programmed cell death protein-1; pfu, plaque-forming units; RNA-seq, RNA sequencing.

not the non-injected side. Lymph nodes on RP1-injected sides were noticeably inflamed and significantly heavier on harvesting 7 days after the first three doses (online supplemental figure S1D). In addition, splenomegaly was observed (online supplemental figure S1E), indicative of an inflammatory response.

To investigate the combination of RP1 with anti-PD-1, intratumoral injections of RP1 were reduced to subtherapeutic levels (three injections instead of six). Here, combination therapy with RP1 and anti-PD-1 delayed tumor growth in both injected and non-injected lesions compared with the single-agent therapies or sham virus and isotype control injections (figure 1B). Attempts to improve these results by combining with other immunomodulatory treatments (anti-TIGIT (T cell immunoreceptor with Ig and ITIM domains), or anti-LAG3 (lymphocyte activation gene 3) antibodies) did not improve efficacy (online supplemental figure S1F,G). Indeed, anti-LAG3 antibodies antagonized the therapeutic efficacy of RP1 alone, and in the case of the injected tumors, RP1 combined with anti-PD-1 (online supplemental figure S1G).

The combination with anti-PD-1 was also tested with the mouse version of RP3. RP3, like RP1, has been engineered with deletion of both copies of ICP34.5 and ICP47 and encodes the GALV-GP-R- fusogenic glycoprotein. However, instead of GM-CSF, RP3 encodes an anti-cytotoxic T-lymphocyte associated protein 4 antibody-like molecule, CD40L and 4-1BBL. While RP3 led to impressive tumor volume reduction in the injected flanks when given by itself, contralateral tumor burden was improved by the addition of anti-PD-1 (figure 1C).

Given our objective of understanding the mechanisms underlying OI combined with other types of immunotherapy, we chose to restrict further analyses to relatively subtherapeutic doses of RP1 and anti-PD-1. Initially, we collected tumors for RNA sequencing (RNA-seq) analysis. This revealed signatures consistent with upregulation of IFN production and responses, T-cell migration, and neutrophil chemotaxis, which were each further increased by the addition of anti-PD-1 (figure 1D,E). Inferred immune cell scoring of RNA-seq data demonstrated a signature indicative of immune cell infiltration into RP1-injected tumors (figure 1F). Interestingly, these RNA-seq analyses also demonstrated similar changes in inflammatory gene expression and predicted cellular infiltration with RP1 alone and RP1 plus anti-PD-1 therapy in contralateral, non-injected tumors (figure 1E,F).

Splenocytes, but not tumor cells, respond to RP1 by upregulating PD-L1 expression

Further detailed analysis of RNA-seq data revealed significant upregulation of genes associated with an IFN response, such as CD274 (PD-L1), chemoattraction and antigen presentation (figure 2A). These responses were confirmed in tumors at the protein level by analysis of cytokines in tumor supernatants, which showed upregulation of IFN-γ and CCL5 7 days after the first of three doses of RP1 (figure 2B).

Next, we investigated the source of the RP1-induced IFN response within tumors. 4434 cells and splenocytes were treated in vitro with RP1 to represent the tumor versus immune cellular compartments. In 4434 cells, RP1 did not elicit type I, II or III IFN expression, in the form of IFN-α, IFN-β, IFN-γ or IL-28, or STAT1 expression. We also measured levels of cGAMP in both cellular and extracellular (supernatant) compartments of tumor cells treated with RP1. No cGAMP was detected, in contrast to the DNA-transfected control (online supplemental figure S2A). In contrast, RP1 induced expression of all these genes, except for IFN-α, in splenocytes demonstrating that RP1 activates the expression of the IFN signature in immune cells (figure 2C).

To determine whether the increased IFN expression in these splenocytes was associated with PD-L1 upregulation, surface expression of PD-L1 was measured over 4–24 hours after RP1 exposure. A perceptible shift in expression (summarized as mean fluorescence intensity) of PD-L1, but not PD-1, was observed over this time frame (figure 2, online supplemental figure S2B,C). To understand whether splenocytes allow for productive replication, a viral growth assay was performed where splenocytes were incubated with RP1 and samples were taken over 48 hours. The amount of virus retrieved was comparable to the amounts in samples containing medium but no cells (online supplemental figure S2D). Taken together, splenocytes appear to respond to RP1 but resist active viral replication. To further understand the interaction between splenocytes and RP1, in a separate experiment, splenocytes were incubated with $RP1^{GFP}$, then washed three times before co-culture on tumor cells. We observed that tumor cells became infected with RP1 via green fluorescent protein (GFP) expression, suggesting RP1 hand-off from splenocytes (online supplemental figure S2E). This phenomenon has been observed in previous studies.[7]

RP1-treated splenocytes initiate a PD-L1 response in tumor cells when co-cultured

Since tumor cells do not exist in isolation from the tumor microenvironment in vivo, we tested whether tumor cell responses to RP1 would be altered in the presence of immune cells by co-culturing 4434 cells with splenocytes. mCherry-expressing tumor cells (4434-mCherry) were used so that, along with staining for CD45, tumor and splenocyte populations could be easily distinguished by gating on these populations in flow cytometry analysis (online supplemental figure S3A). When tumor cells were cultured alone, they did not express PD-L1 in response to RP1, in line with the data presented above. However, when co-cultured with splenocytes, marked upregulation of PD-L1 was observed on tumor cells and this response was dependent on JAK/STAT signaling, as determined by inhibition with ruxolitinib (figure 3A). Since PD-L1 expression on tumor cells could be reversed

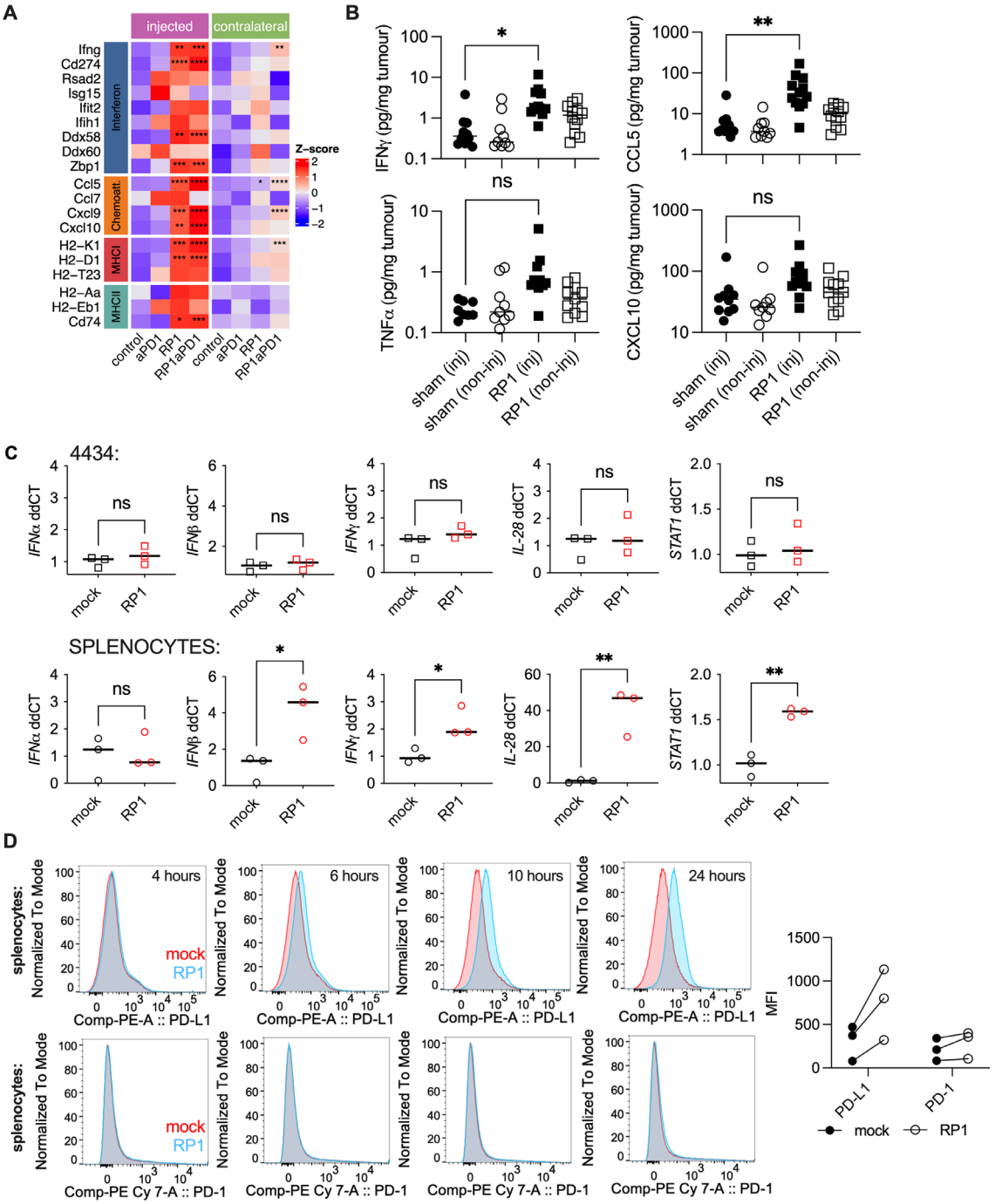

Figure 2 RP1+anti-PD-1 is associated with an IFN signature that can be recapitulated in vitro in splenocytes, but not in tumor cells. (A) Heatmaps corresponding to gene expression from RNA-seq data taken from 4434 tumor samples. Samples were from C57BL/6 mice bearing bi-flank 4434 tumors, injected in one flank with three doses of 5×10^6 pfu RP1 or sham, three doses of anti-PD-1 at 10 mg/kg given I.P., or the combination (concomitantly). Tumors were collected for RNA sequencing analysis day 8 after the first injection. Data represent n=5 tumors per group. P values were determined by a two-tailed t-test, and represent the comparison between each of the treatments against the control. (B) IFN-γ, TNF-α, CCL5 and CXCL10 in supernatants from tumors from C57BL/6 mice bearing bi-flank 4434 tumors. Tumors were injected in one flank with three doses of 5×10^6 pfu RP1 (n=12) or sham injection of formulation buffer (n=10), and collected 7 days after the first RP1 injection. A one-way ANOVA was used with the p value corrected for multiple comparisons. (C) Expression of IFN-related genes in either 4434 tumor cells or mouse splenocytes treated with RP1 by qRT-PCR, at 20 hours after infection. P values were determined by a two-tailed t-test. (D) PD-L1 and PD-1 surface expression in mouse splenocytes treated with RP1 over time by flow cytometry. MFI is shown for three independent repeats at 24 hours after RP1. P values were derived where p>0.05 ns, *p≤0.05, **p≤0.01, ***p≤0.001, ****p≤0.0001. ANOVA, analysis of variance; CCL5, C-C motif chemokine ligand 5; CXCL10, C-X-C motif chemokine ligand 10; IFN, interferon; I.P., intraperitoneal; MFI, mean fluorescence intensity; PD-1, programmed cell death protein-1; PD-L1, programmed death-ligand 1; pfu, plaque-forming units; qRT-PCR, quantitative reverse transcription polymerase chain reaction; RNA-seq, RNA sequencing; TNF, tumor necrosis factor.

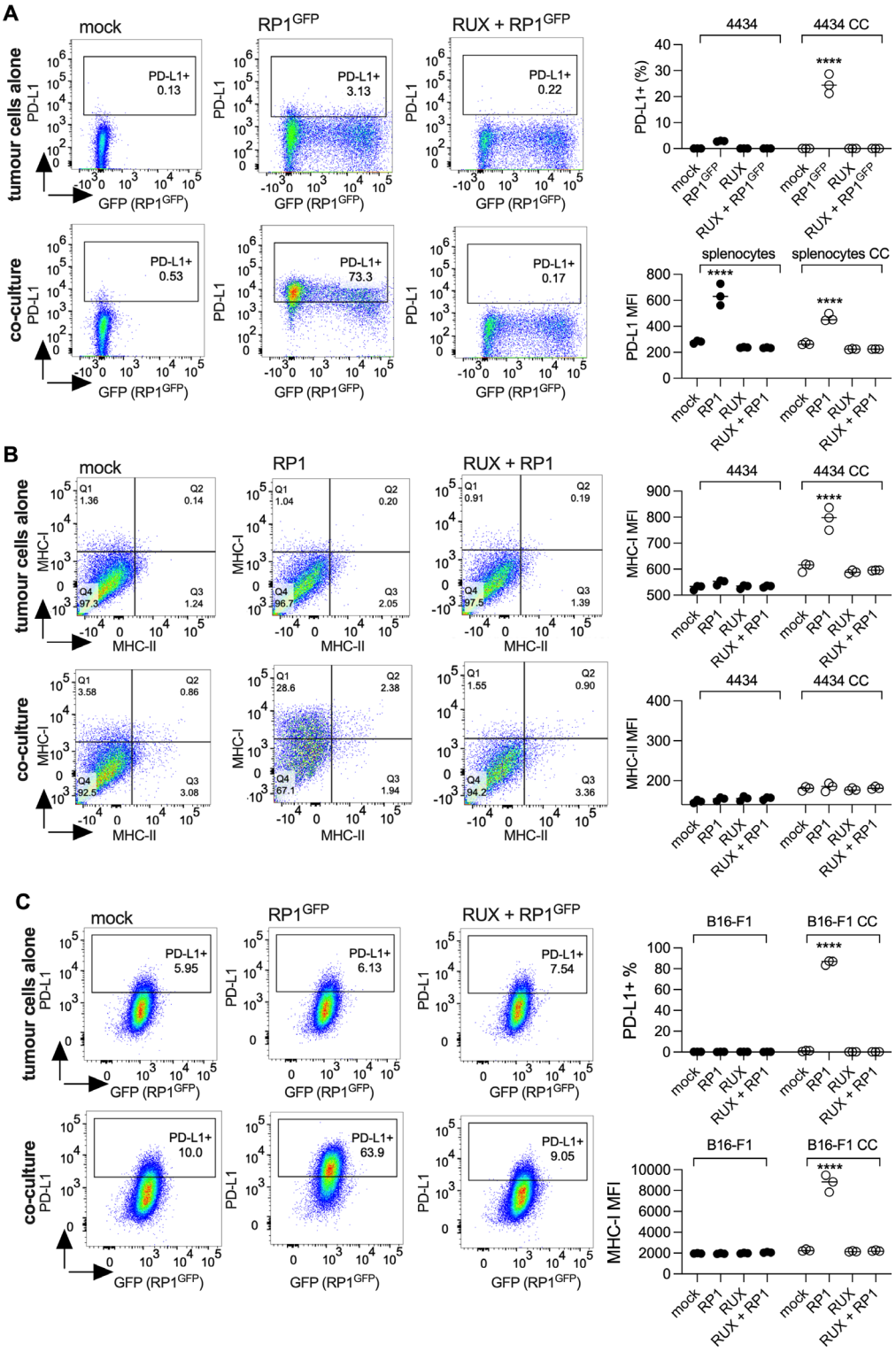

Figure 3 When co-cultured, RP1 treated splenocytes induce PD-L1 expression in tumor cells, which is suppressed by the addition of ruxolitinib. (A) 4434 mCherry tumor cells were co-cultured with or without immune cells, and treated with $RP1^{GFP}$ (MOI 0.01), or $RP1^{GFP}$ with the JAK/STAT inhibitor, ruxolitinib at 1 µM (RUX). Data show expression of GFP+ (that demonstrate cells undergoing virus replication) and PD-L1+ on gated 4434 mCherry tumor cells. (B) MHC-I and MHC-II expression on gated 4434 mCherry tumor cells as described in A. (C) B16 tumor cells were co-cultured with or without immune cells, and treated with $RP1^{GFP}$ (MOI 0.01), or $RP1^{GFP}$ with the JAK/STAT inhibitor, ruxolitinib at 1 µM. Data show a lack of GFP+ expression (demonstrating non-permissiveness of B16 to viral infection) and PD-L1+ and MHC-I expression (MFI) on gated B16 tumor cells out of the co-culture with splenocytes (CC), or tumor cells alone. All gates used in each figure are identical between the samples within them, and all quantitative data shown are for three separate spleens and are representative of at least two independent repeats. CC, co-culture; GFP, green fluorescent protein; MFI, mean fluorescence intensity; MHC, major histocompatibility complex; MOI, multiplicity of infection; PD-L1, programmed death-ligand 1.

by interrupting IFN signaling, we assessed whether effects on MHC-I and MHC-II expression were also affected. Direct infection of tumor cells with RP1 did not alter MHC-I and MHC-II expression (as expected). However, when co-cultured with RP1-exposed splenocytes, tumor cells responded by upregulating MHC-I, but not MHC-II. Again, this effect was dependent on JAK/STAT signaling since it was abrogated by ruxolitinib (figure 3B). Interestingly, induction of PD-L1 expression on tumor cells by co-culture with RP1-exposed splenocytes did not depend on active replication of RP1 within tumor cells (demonstrated by PD-L1 upregulation regardless of the presence of GFP (encoded within RP1) in the tumor cell, figure 3A). To demonstrate that these effects were independent of the tumor cells' capacity to support RP1 replication, the non-permissive B16 cell line was used instead of 4434 in co-culture experiments. In these experiments, similar results were observed. PD-L1 expression was increased in B16 cells only when they were co-cultured with RP1-exposed splenocytes. As expected, there was no GFP production from $RP1^{GFP}$ in RP1-treated B16 cells. As with 4434 cells, PD-L1 expression on B16 cells returned to baseline with ruxolitinib (figure 3, online supplemental figure S3B). Taken together, these results highlight the role of immune cell populations in mediating IFN responses to RP1 which, in turn, can upregulate PD-L1 and MHC-I expression on tumor cells.

IFNAR1 k/o splenocytes do not express PD-L1 in response to RP1 and do not induce PD-L1 expression on tumor cells in co-culture

In light of the data highlighting the role of splenocytes in mediating responses to RP1 that tumor cells could not elicit alone, we investigated effects with splenocytes from IFNAR1 and TNFAR1 receptor knock-out (k/o) mice. We used IFNAR1 and TNFAR1 k/o splenocytes, since these receptors play roles in anti-viral responses. We first addressed evidence of RP1 replication in splenocytes and whether, given that these receptors are central to orchestrating an anti-viral response, loss of these might render splenocytes permissive to RP1 replication. This was not the case. In wild-type, IFNAR1 or TNFAR1 k/o splenocytes, we did not observe RP1 replication, assessed via the production of GFP using $RP1^{GFP}$ virus (online supplemental figure S4A,B), demonstrating the inability of RP1 to replicate in splenocytes.

Next, we looked at the response of splenocytes to RP1 when the splenocytes were cultured alone. The RP1-induced increase in PD-L1 expression on wild-type splenocytes was reduced in IFNAR1 k/o splenocytes. Interestingly, TNFAR1 k/o splenocytes showed a modest increase over that seen with wild-type splenocytes (figure 4A,B). We extended the use of these k/o splenocytes to co-culture experiments with 4434-mCherry cells. The induced expression of PD-L1 and MHC-I on tumor cells co-cultured with RP1-exposed splenocytes was unaltered between wild-type and TNFAR1 k/o splenocytes (figure 4C). However, tumor cells co-cultured with RP1-treated IFNAR1 k/o splenocytes did not upregulate PD-L1 and MHC-I to the extent that was observed with wild-type splenocytes (figure 4D). The attenuation of IFNβ production in response to RP1 was demonstrated in IFNAR1 k/o splenocytes by ELISA (online supplemental figure S4C). Treatment of 4434 cells with IFN-β and IFN-γ, but not tumor necrosis factor (TNF)-α, induced expression of PD-L1 and MHC-I, supporting the notion that IFN-driven, but not TNF-α-driven, responses play a role in upregulating PD-L1/MHC-I expression on tumor cells, and corroborating the results seen in experiments using the k/o splenocytes (figure 4E).

STING is critical in mediating the IFN response to RP1

Data so far indicated a strong involvement of the IFN response via JAK/STAT signaling in mediating the effects of RP1 on PD-L1 expression. To interrogate upstream elements of this response, we focused on the effects on the cytosolic DNA sensor, cGAS, and its effector, STING. Since RP1 is a double-stranded DNA virus, we surmised that STING signaling in immune cells was the most likely mediator of the IFN responses to RP1. To test this, we used splenocytes derived from STING k/o mice. As with the wild-type, TNFAR1 k/o, and IFNAR1 k/o splenocytes, STING knock-out splenocytes were non-permissive to $RP1^{GFP}$ replication (online supplemental figure S5A).

The increase in PD-L1 expression induced on wild-type splenocytes with RP1 was absent in STING k/o splenocytes (figure 5A). When tumor cells were co-cultured with RP1-exposed STING k/o splenocytes, they failed to upregulate PD-L1 or MHC-I to the same extent as wild-type (figure 5B). Taken together, these data highlight the role of STING in orchestrating responses to RP1 in immune cells.

Subsequently, we tested if the observed tumor responses to RP1-exposed splenocytes required cell–cell contact. To address this question, splenocytes and tumor cells were separated by a 0.4 µM membrane in a transwell assay. Despite this prevention of cell–cell contact, tumors were still able to respond to immune cells that had been exposed to RP1 by upregulating PD-L1 (figure 5C).

To confirm that these effects were independent of tumor cell-virus interaction (from RP1 diffusing from the splenocyte compartment), tumor cells were incubated with supernatants from RP1-treated splenocytes that had been passed through a 0.1 µM filter. The ability of this filter to prevent the passage of RP1 was tested against filters of other sizes (online supplemental figure S5B). The absence of RP1 also was confirmed in the experiment by gating on GFP for $RP1^{GFP}$, and checking that no GFP expression was seen in the sample. Again, tumor cells responded to the filtered supernatants by upregulating PD-L1, indicating that the tumor cells are likely responding to a secreted signal released by RP1-exposed splenocytes (figure 5D). Finally, tumor cells were treated with filtered supernatants from RP1-treated splenocytes in the presence of ruxolitinib. This prevented expression

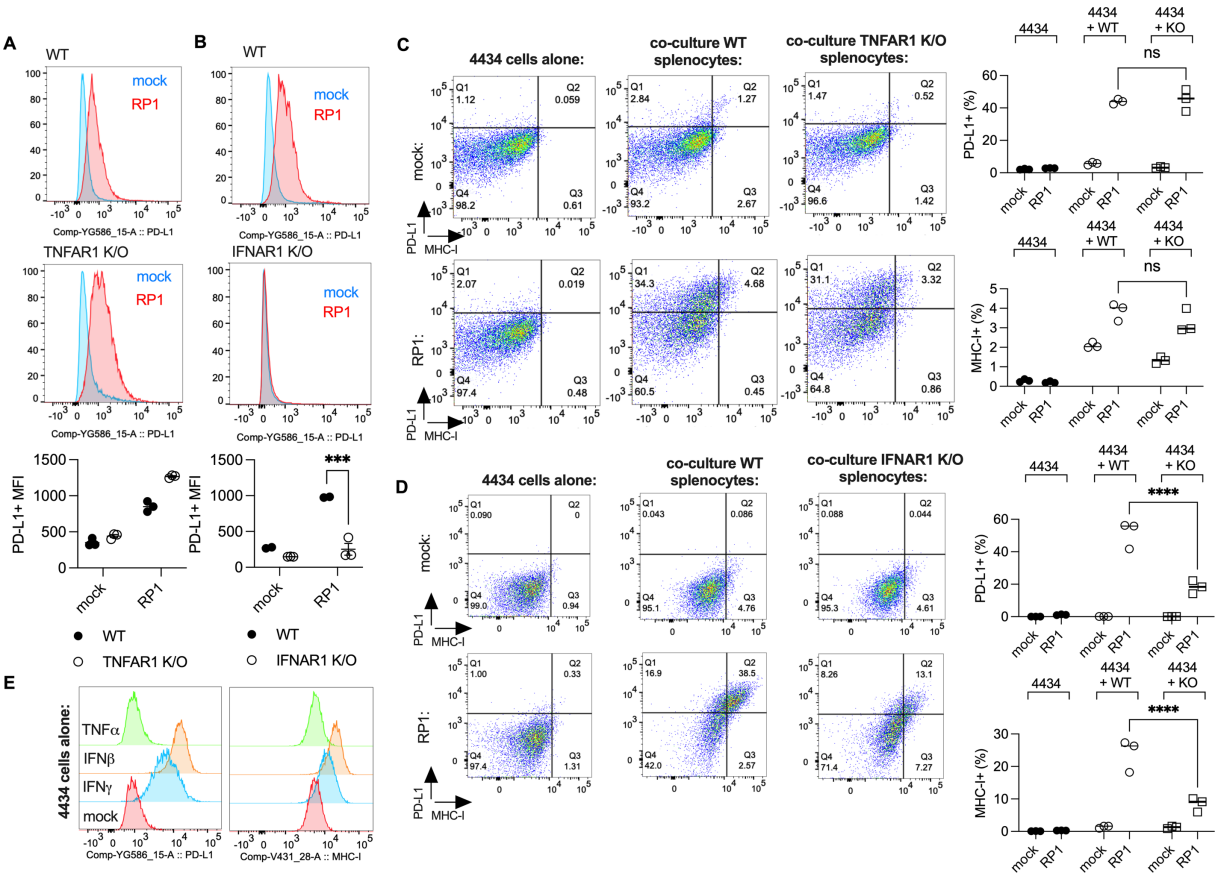

Figure 4 IFNAR1 k/o splenocytes are not able to respond to RP1 via upregulation of PD-L1, and do not induce PD-L1 expression in tumor cells. (A) PD-L1 expression in TNFAR1 WT versus TNFAR1 k/o splenocytes treated with RP1. Data show representative histograms and MFI for n=3. (B) PD-L1 expression in IFNAR1 WT versus IFNAR1 k/o splenocytes treated with RP1. Data show representative histograms and MFI for n=3. (C) PD-L1 and MHC-I expression in 4434 mCherry tumor cells cultured either alone, or in co-culture with WT or TNFAR1 k/o splenocytes, treated with RP1. Representative plots are shown and % PD-L1+ and MHC-I+ populations from the 4434 mCherry compartment are shown for n=3 experiments. (D) PD-L1 and MHC-I expression in 4434 mCherry tumor cells cultured either alone, or in co-culture with WT or IFNAR1 k/o splenocytes, treated with RP1. Representative plots are shown and % PD-L1+ and MHC-I+ populations from the 4434 mCherry compartment are shown for n=2 experiments. (E) 4434 cells treated with 20 ng/mL of IFN-β, IFN-γ or TNF-α for 24 hours and measured for PD-L1 and MHC-I expression by flow cytometry. Data are representative of two independent repeats. IFN, interferon; k/o, knock-out; MFI, mean fluorescence intensity; MHC, major histocompatibility complex; PD-L1, programmed death-ligand 1; TNF, tumor necrosis factor.

of PD-L1 on tumor cells, confirming that the tumor cells respond via intrinsic JAK/STAT signaling (figure 5E).

To probe the effects of STING on the cytokines released from RP1-exposed splenocytes further, we performed a LEGENDplex assay. With STING k/o splenocytes, RP1 exposure did not induce IFN-α/β/γ, CCL5 or CXCL10 release to levels observed from wild-type splenocytes (figure 5, online supplemental figure S5C). There were no differences in the secretion of IL-10, IL-12, IL-1β or CXCL1 between RP1-treated and non-treated splenocytes (data not shown). There were also no changes in levels of GM-CSF between RP1-treated and non-treated splenocytes. Since GM-CSF is encoded by RP1, the unchanged levels likely reflect a lack of RP1 replication and subsequent transgene expression within these cells, as expected (online supplemental figure S5C).

In summary, these data demonstrate that, in immune cells, STING has a role in viral sensing that can be broadcast to tumor cells via secreted cytokines, resulting in upregulation of MHC-I and PD-L1 on tumor cells.

Neutrophils infiltrate the tumor after RP1 injection and express PD-L1

Next, we asked how the responses seen in vitro reflect what occurs in vivo. Flow cytometry analysis of a bi-flank 4434 tumor model, in which tumor was injected only on one side, showed high levels of PD-L1+cells only within the RP1-injected tumor and at 8 days after the first of three RP1 injections (figure 6, online supplemental figure S6A). On flow cytometry analyses, PD-L1+cells from tumors were backgated and 80.9% stained positively for CD11b and Ly6G, characteristic of neutrophils (figure 6B). T-distributed stochastic neighbor embedding (t-SNE) analysis of myeloid populations also demonstrated an influx of neutrophils in RP1 injected tumors (figure 6, online supplemental figure S6B), and these corresponded with

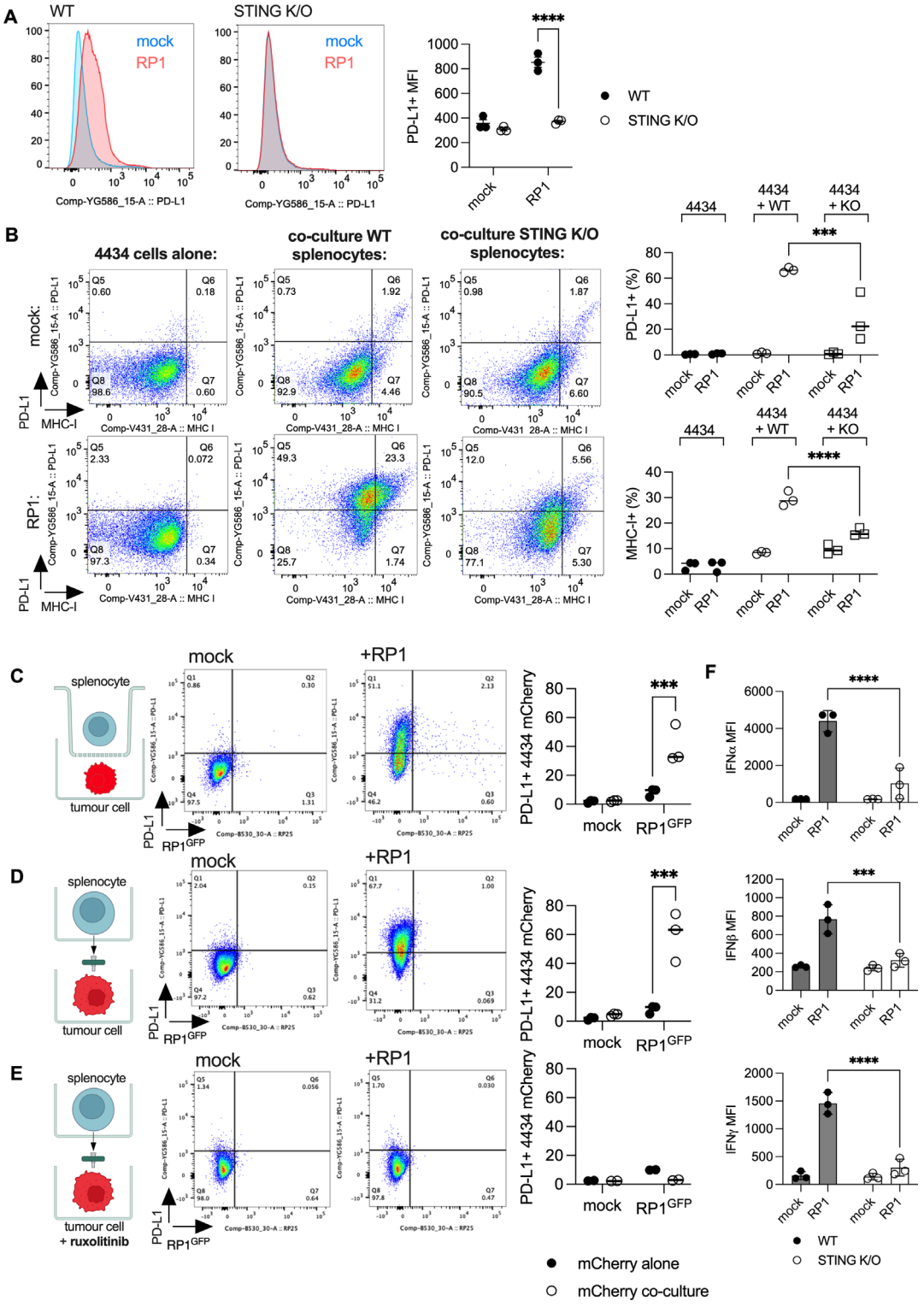

Figure 5 The IFN responses to RP1 in splenocytes are mediated through STING. (A) PD-L1 expression in WT versus STING k/o splenocytes, treated with RP1. Data show representative histograms and MFI for n=3. (B) PD-L1 and MHC-I expression in 4434 mCherry tumor cells cultured either alone or gated out from co-culture with WT or STING k/o splenocytes, treated with RP1. Representative plots are shown and % PD-L1+ and MHC-I+ populations from the 4434 mCherry compartment are shown for n=3 experiments. (C) PD-L1 expression in 4434 mCherry tumor cells co-cultured with immune cells for 24 hours, separated by a transwell. (D) Splenocytes were treated with or without RP1 for 24 hours, and supernatants were passed through a 0.1 µm filter before transfer to 4434 mCherry cells. PD-L1 expression in 4434 mCherry cells was measured by flow cytometry. (E) As in D, but the supernatants were transferred to 4434 mCherry cells and 1 µM ruxolitinib was added to the tumor cells. Data form C–E show representative plots and quantitative data from three spleens. (F) IFN-α, IFN-β, and IFN-γ in supernatants taken from either WT or STING k/o splenocytes treated with RP1. IFN, interferon; k/o, knock-out; MFI, mean fluorescence intensity; MHC, major histocompatibility complex; PD-L1, programmed death-ligand 1.

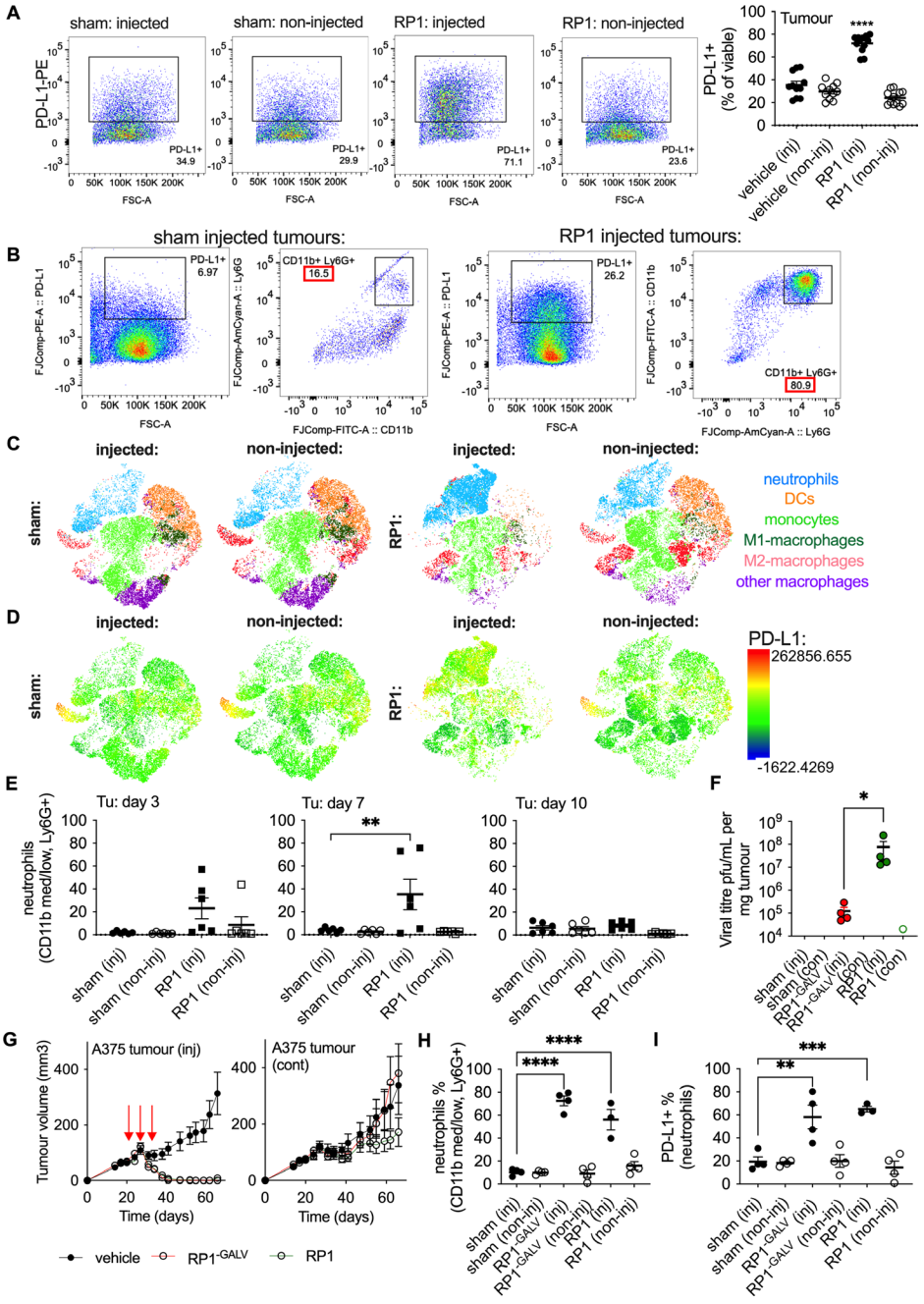

Figure 6 In an in vivo setting, neutrophils upregulate PD-L1 in response to RP1, which are abundant within the CD45 population. (A) C57BL/6 mice bearing bi-flank 4434 tumors were injected in one flank with three doses of 5×10^6 pfu RP1. Tumors were harvested 8 days after the first injection and stained for PD-L1. A one-way ANOVA was used with the p value corrected for multiple comparisons. (B) Backgating on PD-L1+cells reveals a high proportion to be CD11b+Ly6G+in RP1 treated tumors versus sham injected. Data are concatenated from n=6 tumors collected 8 days after the first injection of treatment as described in A. (C) t-SNE plots show myeloid compartments for tumors treated as described in A. (D) Respective PD-L1 expression for relative t-SNE plots shown in B. (E) C57BL/6 mice bearing bi-flank 4434 tumors were injected in one flank with three doses of 5×10^6 pfu RP1 and were collected at various time points and stained for CD11b+ and Ly6G+ from viable CD45+ populations. A one-way ANOVA was used with the p value corrected for multiple comparisons made between injected and non-injected tumors. (F) CD1 nude mice bearing bi-flank A375 tumors were injected on one side with three injections of RP1 or RP1^{-GALV}. Tumors were harvested at day 8 after the first dose of virus (n=4 per group). Supernatants from the tumors were analyzed for viral load by $TCID_{50}$ assay on BHK cells. P values were determined by a two-tailed t-test between injected tumors with RP1 and RP1^{-GALV}. (G) Tumor volumes from CD1 nude mice bearing bi-flank A375 tumors, injected in one side with three injections of RP1 (n=7), RP1^{-GALV} (n=8), or sham injection of formulation buffer (n=7). (H) CD1 nude mice bearing bi-flank A375 tumors were injected in one side with three injections of RP1 or RP1^{-GALV}. Tumors were harvested 8 days after the first injection and stained for neutrophil infiltrate (CD11b+, Ly6G+). (I) As in H, tumors were harvested 8 days after the first injection and stained for PD-L1+expression on the neutrophil population (CD11b+, Ly6G+). ANOVA, analysis of variance; DCs, dendritic cells; PD-L1, programmed death-ligand 1; pfu, plaque-forming units; t-SNE, t-distributed stochastic neighbor embedding.

PD-L1-high expressing cells (figure 6D). A time course experiment revealed a time-limited infiltration of neutrophils into RP1-injected tumors that was initiated by 2 days after the first dose of RP1 (day 3), persisted at day 7, but resolved by day 10 (figure 6E).

To explore the role of myeloid cells in RP1 therapy further, we used T cell-deficient CD1 nude mice bearing human A375 melanoma bi-flank tumors. Since human cells but not mouse cells express the pit-1 receptor, which is required for the binding of GALV fusogenic protein and generation of cell–cell fusion and syncytium formation, we took this opportunity to study the effects of GALV-GP R- expression from RP1. These viruses are detailed as previously described by Thomas *et al*, and referred to as virus 16 and virus 19 in this study, but RP1 and RP1^{-GALV} herein[6] (online supplemental figure S6C). RP1 revealed superior killing in the A375 melanoma human cell line in vitro (online supplemental figure S6D). Animals received intratumoral treatment with a GALV-GP R-expressing or non-expressing version of RP1 in a direct comparison. Detection of RP1 was largely restricted to injected tumors, with an increase in virus titers seen with the GALV-GP R- expressing, as opposed to the non-expressing virus (figure 6F), with both viruses resulting in cures in the injected tumors (figure 6G). As seen in the 4434-bearing C57BL/6 model, we also observed a predominant infiltration of Ly6G+, CD11b+ neutrophil subsets in RP1-injected tumors, which was independent of whether or not the virus expressed GALV-GP R- (figure 6H). No such changes were observed for monocytes, Dendritic cells (DCs), macrophages, natural killer or B cells (online supplemental figure S6E). Furthermore, these tumor-infiltrating neutrophils expressed high levels of PD-L1 (figure 6I). Finally, to address whether neutrophils are likely able to respond to RP1 exposure directly through upregulation of PD-L1, or whether the presence of other immune cells is required, neutrophils were isolated from the bone marrow of C57BL/6 mice and treated with RP1. These immature neutrophils upregulated PD-L1 expression in response to RP1, suggesting that these cells can detect and respond to the virus without a reliance on signals emitted from other cells (online supplemental figure S6F,G). However, it is worth noting that a slight upregulation in PD-L1 expression was also seen in CD3+cells within tumors that received RP1 injections, in vivo (online supplemental figure S6H). In vitro, PD-L1 was upregulated on CD3+cells gated out from the total RP1-exposed splenocyte (online supplemental figure S6I). Therefore, other immune populations appear to be capable of upregulating PD-L1 in response to RP1; however, neutrophils are a predominant population found in tumors treated with RP1 in vivo.

DISCUSSION

The immune checkpoint protein, PD-L1, delivers inhibitory signals to restrain T-cell activity when expressed on the surface of cells.[8] While critical in preventing auto-immune diseases and maintaining tolerance to self antigens, many cancers commandeer this signaling mechanism to evade immune system responses.[9] PD-L1 is also expressed as part of a normal host response to many viral infections, largely driven by anti-viral IFN responses.[10] Therapeutic targeting of the PD-L1/PD-1 axis (with a growing number of approved anti-PD-1 and anti-PD-L1 monoclonal antibodies) in combination with OIs is currently being explored in many clinical trials.[11] Therefore, it is important to understand the clinical responses achieved in the broader context of cross-talk between all virally exposed elements within the immune tumor microenvironment. Furthermore, an understanding of the identities of the cells within this microenvironment that express PD-L1 in response to OIs would improve both the mechanistic understanding of any therapeutic gain and help in determining the dominant immune-suppressive axes within the tumor. Such information might usefully inform and tailor selection of appropriate combination therapeutic partners.

In this study, we observed induced expression of IFN-stimulated genes in murine tumors in vivo by RNA-seq analysis. While other OIs in other cell types can induce IFN responses directly in tumor cells in vitro, this was not observed in our 4434 melanoma model with RP1.[12] In contrast, murine splenocytes cultured in vitro responded to RP1 exposure through upregulation of type I and type III IFNs, and with the upregulation of surface expression of PD-L1. Despite this lack of IFN response in the murine 4434 melanoma tumor cell line or, indeed, perhaps because of it, these cells were permissive to RP1 replication, shown by increases in virus-encoded GFP expression that was not evident in splenocytes. Interestingly, even the loss of STING, TNF-α, or IFNAR1 in k/o splenocytes was not sufficient to allow RP1 replication to proceed, underlining the robust tumor-selective mechanisms that have been engineered into RP1 to prevent its replication in non-malignant tissues. Loss of IFNAR1 or STING did, however, interfere with the ability of the splenocytes to express PD-L1 in response to exposure to RP1. Additionally, IFN expression was not induced in these k/o splenocytes to the levels seen in wild-type splenocytes. The interaction between splenocytes is not yet fully understood. They do not appear to support viral replication, although there may be some limitations in the assays used in this study. It is impossible to exclude the possibility that a cell type in low levels of abundance does allow replication to an extent that is not detectable in the assays we have employed. While it does seem that splenocytes are able to respond to RP1 through the observed IFN responses, it is not yet certain exactly how the virus activates STING. These questions will be explored in future work.

Although experiments on isolated tumor cell and splenocyte populations were informative, it is important to remember that tumor and immune cells do not exist in separate compartments within the tumor. Therefore, in order to reflect this reality in vitro, we investigated the

tumor cell response to the IFNs released by RP1-treated splenocytes. This was explored by co-culture assays using mCherry-tagged 4434 cells so they might be isolated and studied through selective gating in flow cytometry analyses. Despite an inability of tumor cells to upregulate PD-L1 in response to RP1 infection directly, they were able to upregulate PD-L1 when co-cultured with RP1-exposed splenocytes. Importantly, we demonstrated that this mechanism was not governed by cell-to-cell contact (ie, touch), but through a secreted signal, since tumor cells were still able to respond (with PD-L1 upregulation) when they were separated from the splenocytes in a transwell system, or treated with filtered (virus-free) splenocyte-conditioned media.

These data highlight the importance of the immune cell component of the microenvironment in mediating clinical responses to OI. It is noteworthy that similar effects were observed using the murine B16 melanoma cell line, which is non-permissive to viral replication. Despite a lack of virus replication in B16 cells, when co-cultured with splenocytes, they were still able to respond through upregulation of PD-L1 expression. Clearly, this observation has important implications for the clinical development of RP1; patients with lesions that are resistant to RP1 infection and/or replication might still benefit from treatment through immune cell-mediated viral sensing and reconditioning of the tumor-immune microenvironment to a more immune-responsive phenotype.

Given the documented changes in the tumor-immune microenvironment, we were keen to understand the specific immune subsets that were contributing to the observed effects on PD-L1 expression in the TME in vivo. We observed a marked influx of CD11b+Ly6G+neutrophils into injected tumors that was seen in both immunocompetent (C57BL/6) and immunodeficient (CD1 nude) mouse models. In each, neutrophils infiltrating the injected tumors expressed high levels of PD-L1. A limitation of our in vivo studies was the need to select time points at which to take snapshots of the tumor microenvironment and, thus, it is possible that we may not have captured the full picture of the response to RP1. Indeed, it is conceivable that other immune (and non-immune) cell populations may also upregulate PD-L1 in response to RP1. Perhaps our data reflect the fact that neutrophils are the most abundant, and relatively short-lived, innate immune cell or migrate early to virus-treated tumors.[13] Nonetheless, these data put neutrophils in the spotlight as a cell type to target in future combination approaches.

Neutrophils can display both procancer and anticancer functions, depending on context.[14] They have been implicated in tumor cell kill through phagocytosis, granule release, and neutrophil extracellular traps.[15] They can also support inflammatory responses to the tumor. However, they are also implicated in immunosuppression through downregulation of T-cell responses.[16 17] Our data suggest that RP1 induces an influx of neutrophils to the tumor microenvironment, the majority of which are PD-L1+ and, as such, likely to exert immuno-suppressive effects. Since the combination of RP1 plus anti-PD-1 therapy led to improvements in therapeutic efficacy, in both injected and non-injected tumors, it would be interesting to investigate other receptors that are expressed on immune subsets, such as neutrophils and macrophages, in response to virus. An understanding of how these communicate with key components of the adaptive immune response, such as T cells, in orchestrating an effective antitumor immune response will hopefully drive discoveries of other potentially suppressive receptors that can be targeted.

In conclusion, we have demonstrated that viral OIs exert complex effects within the tumor-immune microenvironment and demonstrated changes in gene expression in immune cell gene signatures both in the injected and non-injected tumors. Further, we highlight the fact that, in addition to their direct, replication-mediated, cytotoxic effects on tumor cells, RP1 can communicate with immune cell compartments within the tumor and these effects can be broadcast more widely to tumors. Importantly, this cross-talk with immune cells within the tumor microenvironment does not require active viral replication. These findings point towards future studies in which both the cytotoxic, tumor cell-autonomous and the non-cytotoxic, immunomodulatory effects within the tumor microenvironment can be exploited to maximize responses in both injected and non-injected lesions.

Materials and methods

In vivo experiments

All procedures were approved by the Animal Welfare and Ethical Review Board at the Institute of Cancer Research in accordance with Home Office Regulations under the Animals (Scientific Procedures) Act 1986. All animals were handled according to the Institute and UK Home Office guidelines and kept in a pathogen-free facility and exposed to a 12-hour light/dark cycle at a constant temperature (22±2°C), with access to unrestricted food and water supply. CD1 nude mice or C57BL/6 mice (female, aged 6–8 weeks, Charles Rivers, Kent, UK) received subcutaneous injections of 3×10^6 A375 cells or 4×10^6 4434 cells, respectively, in the right and left flanks. Once tumors had grown to ~6 mm in diameter, mice were allocated to treatment groups balanced by tumor size for subsequent treatment. Cages were used as experimental units, and sample size was calculated through previous experiments. Virus injections of 5×10^6 plaque-forming units dissolved in formulation buffer (or a formulation buffer sham) were administered intratumorally. Therapeutic antibodies: anti-PD-1 antibody (RMPI-14 – BE0146) or isotype control (IgG2a 2A3 – BE0089); anti-TIGIT antibody (1G9 – BE0274) or isotype control (IgG1 – BE0083); anti-LAG3 antibody (C9B7W – BE0174) or isotype control (HRPN – BE0088); anti-CD25 (PC61, SG3249) or isotype control (Bio X Cell) were administered at 10 mg/kg by intraperitoneal injection. All antibodies were resuspended in IP0070 InVivoPure pH 7.0 dilution buffer. Established tumor volumes

were measured at least two times per week using Vernier calipers and the tumor volume was estimated from the formula: V=0.5×(length×width^2). Permission was granted to perform animal experiments according to Home Office, with animals judged to have failed treatment if tumor diameter approached the size limit of 15 mm in one of three dimensions. These limits were adhered to in all experiments. The humane endpoint was euthanasia by neck dislocation due to moribund status as determined by weight loss of 18% or more compared with maximum weight measured, inability to reach food or water, breathing difficulties, hunched intermittently, anorexia, dehydration, marked piloerection, lethargy and subdued. Animal weights were monitored two times per week.

RNA sequencing

4434 tumors were treated with three injections of virus each given a day apart and harvested for RNA-seq 3 days after the last virus injection. RNA from tumors was extracted and purified using the RNeasy plus extraction kit (Qiagen, 74134). Library preparation and sequencing were performed by GENEWIZ (Leipzig, Germany). Library prep was strand-specific, with PolyA selection and 2×150 bp sequencing at 10 million pairs performed on an Illumina NovaSeq. Quantification of transcripts expression was performed using Salmon quant V.1.10.1 (https://www.nature.com/articles/nmeth.4197) against GRCm39 mouse reference (Ensembl release 103) and aggregated to gene level using tximport V.1.34 R package (https://f1000research.com/articles/4–1521/v1). DESeq2 package (https://genomebiology.biomedcentral.com/articles/10.1186/s13059-014-0550-8) was used for differential gene expression analysis (pseudogenes and ribosomal genes were excluded and only genes with count values above 10 in at least five samples were kept for the downstream analysis). Cell type gene signatures (https://www.sciencedirect.com/science/article/pii/S1535610821002221) scores were calculated using GSVA (V.2.0.4) (https://bmcbioinformatics.biomedcentral.com/articles/10.1186/1471-2105-14-7) applied to VST-normalized gene counts. Gene Set Enrichment Analysis for Gene Ontology biological processes terms was performed using clusterProfiler (V.4.14.4).

Immune profiling of tumors

Tumors were harvested and finely minced with scissors prior to the addition of digestion mix (0.01% trypsin, 2.5 mg/mL collagenase type VI (Sigma-Aldrich), 2 mg/mL dispase (Sigma-Aldrich), and 1 mg/mL DNAse type I (Roche) in RPMI (Roswell Park Memorial Institute medium), and incubated at 37°C for 30 min. Thereafter, samples were kept on ice. Suspensions were passed through a 70 µm strainer using a 2.5 mL syringe plunger and washed through with RPMI with 5 mM EDTA until only connective tissue remained. Samples were centrifuged at 1,500 rpm, for 5 min at 4°C, and transferred into a V-well 96-well plate. Samples were Fc blocked (553142, 1:100) for 10 min and stained with extracellular antibodies in FACS buffer (phosphate-buffered saline (PBS)+5% fetal calf serum (FCS)) for 30 min on ice and protected from light. Subsequently, cells were washed in FACS buffer, permeabilized and stained with intracellular antibodies using the Foxp3 transcription Factor Staining Kit (Thermo Fisher Scientific). Samples were then washed and fixed with 1–2% paraformaldehyde (PFA) prior to analysis of tumor-infiltrating lymphocytes by flow cytometry. Samples were analyzed on an LSR II or FACSymphony A5 (BD biosciences) and flow cytometry analyses were performed using FlowJo. Refer to online supplemental table S2 for the details of all the antibodies used.

qRT-PCR experiments

RNA was extracted from samples using RNeasy plus extraction kit (Qiagen, 74134), and complementary DNA (cDNA) was synthesized using SensiFAST cDNA synthesis kit (BIO-65053, Bioline) before amplification against transcripts by quantitative reverse transcription polymerase chain reaction (qRT-PCR) kit with SYBR green (Bioline, BIO-92020). Refer to online supplemental table S1 for primer sequences. Relative gene expression was calculated with the 2-ddCT method using 18S or beta-actin as a housekeeping gene.

Viral replication assays

Tumors were harvested, disaggregated, digested, strained and centrifuged as per details in Immune profiling of tumors (above). The supernatants were titrated on BHK cells for TCID50 assay. Viral titer was calculated by T=101+d(S–0.5), where T=titer, d=LOG(dilution) of sample across BHK cells, S=score. The score was determined by visualization of wells displaying cytopathic effect (CPE). Cells positive for CPE were scored 1 for that dilution. If no CPE was observed, the dilution received a score of 0. Each dilution consisted of triplicate repeats.

Co-culture experiments

Splenocytes from C57BL/6 mice (Charles Rivers, Kent, UK), C57BL/6-*Tnfrsf1a*^{tm1Imx}/J (https://www.jax.org/strain/003242#), B6(Cg)-*Ifnar1*$^{tm1.2Ees}$/J (https://www.jax.org/strain/028288), or B6(Cg)-*Sting1*$^{tm1.2Camb}$/J (https://www.jax.org/strain/025805) were processed immediately by passing through a 70 µm cell strainer using a 2.5 mL syringe plunger, and washed through with cold RPMI (10% (v/v) FCS, 1% (v/v) glutamine, and 0.5% (v/v) penicillin/streptomycin, ICR, CSSD, UK). Cells were spun down at 300×g (1,500 rpm), at 4°C for 2 min. Pellets were resuspended in 1–2 mL of (neat) ACK buffer to destroy red blood cells, followed by neutralization with the addition of 8 mL of cold RPMI. Cells were spun down again, re-suspended in RPMI and passed through a second cell strainer to remove any residual debris/fat. Splenocytes were counted and plated in 12-well plates at 2×10^6, or added to previously plated tumor cells (plated at 2×10^5 per well the night before) in 1 mL per plate. Therefore, the splenocyte: tumor cell ratio was 10:1.

Splenocytes, or the splenocyte-tumor mix were treated with viruses at an multiplicity of infection (MOI) of 0.01 per splenocyte (or 40,000 particles of virus per well), with or without 1 µM ruxolitinib. At the desired time point, samples were harvested, via gently scraping the cells and spun down into Eppendorf tubes. At this point, supernatants were collected for cytokine analysis. Cell pellets were blocked in Fc blocker (553142, 1:100) made up in FACS buffer and blocked for 5–10 min. Cells were then spun down and the Fc block removed. The extracellular antibody mix was then added and incubated on ice and protected from light for 30 min. Cells were then washed in FACS buffer and fixed in 100 µL of fluorofix fixation buffer (BioLegend, 422101) and incubated at 4°C for 30 min. Samples were resuspended in 1 mL of PBS and filtered prior to reading the samples on an LSR II or FACSymphony A5 (BD biosciences). Flow cytometry analyses were performed using FlowJo. Refer to online supplemental table S2 for the details of all the antibodies used.

LEGENDplex cytokine experiments

Supernatants were analyzed for the LEGENDplex multi-analyte flow assay kit (740622, mouse Anti-Virus Response Panel, 13-plex, BioLegend), as per manufacturer's instructions. Samples were read using an FACSymphony A5 (BD Biosciences). Analyses were performed using LEGENDplex software.

Statistical analysis

For in vivo experiments, the area under the curve was calculated for each mouse and the total areas for each treatment group were then tested for normality and lognormality using the Shapiro-Wilk test. If it passed normality, a one-way analysis of variance using parametric was used. If not, the non-parametric test was used. Each treatment group was compared with sham injection.

Author affiliations
[1]The Institute of Cancer Research, London, UK
[2]Replimune Inc, Woburn, Massachusetts, USA
[3]Molecular Medicine, Mayo Clinic, Rochester, Minnesota, USA

Acknowledgements This work was supported by the Institute of Cancer Research/Royal Marsden Hospital Centre for Immunotherapy of Cancer and the CRIS Cancer Foundation. We acknowledge the Flow Cytometry Facility at The Institute of Cancer Research for providing expert support on flow cytometry analysis and cell sorting. Their support was instrumental in achieving the results presented in this paper https://doi.org/10.5281/zenodo.14845954.

Contributors VR, JK, EA, PKB, CZ, AM, RSC and KJH contributed to the conception and design of the research as well as in writing the manuscript; VR, JK, EA, RP and LH performed the in vitro experiments and acquired data; SJ and LK performed the in vitro work on manufacturing the viruses used in this study; RP, NM, CM, JG, DM, MMcL, RV, AM, RSC and KJH contributed to the analysis and interpretation of the data; AP, MMcL and JG provided support for bioinformatics analysis; CCWH, SF, HB, AW, IL, HS, ID, ECP and MP performed and supported in vivo experiments; MG, SL, JM, WF and PM provided support for the in vivo experiments using knockout mice. KJH is the guarantor for the project.

Funding CRUK and Replimune, Inc provided funding for this work. The funder did not influence the results/outcomes of the study despite author affiliations with the funder.

Competing interests RSC, PKB, SJ and LK are employees of Replimune, Inc.

Patient consent for publication Not applicable.

Ethics approval Not applicable.

Provenance and peer review Not commissioned; externally peer reviewed.

Data availability statement All data relevant to the study are included in the article or uploaded as supplementary information.

ORCID iDs
Victoria Roulstone https://orcid.org/0000-0003-4141-8123
Anton Patrikeev https://orcid.org/0009-0000-0638-8390
Charleen ML Chan Wah Hak https://orcid.org/0000-0002-6386-5699
Robert Pickering https://orcid.org/0000-0003-3332-9868
Christian Zierhut https://orcid.org/0000-0003-3501-603X
Lisa C Hubbard https://orcid.org/0009-0007-1540-4445
Isaac Dean https://orcid.org/0000-0002-4750-5335
Emmanuel Christian Patin https://orcid.org/0000-0001-5390-5733
Jim Gkantalis https://orcid.org/0009-0006-0693-2011
Malin Pedersen https://orcid.org/0000-0003-1887-733X
Martin McLaughlin https://orcid.org/0000-0002-9739-7133
Jonathan Mannion https://orcid.org/0000-0001-6054-3451
Alan Melcher https://orcid.org/0000-0002-2042-3380
Kevin J Harrington https://orcid.org/0000-0002-6014-348X

REFERENCES

1 Kaufman HL, Kohlhapp FJ, Zloza A. Oncolytic viruses: a new class of immunotherapy drugs. *Nat Rev Drug Discov* 2015;14:642–62.
2 Bommareddy PK, Shettigar M, Kaufman HL. Integrating oncolytic viruses in combination cancer immunotherapy. *Nat Rev Immunol* 2018;18:498–513.
3 Andtbacka RHI, Kaufman HL, Collichio F, *et al*. Talimogene Laherparepvec Improves Durable Response Rate in Patients With Advanced Melanoma. *J Clin Oncol* 2015;33:2780–8.
4 Chesney JA, Ribas A, Long GV, *et al*. Randomized, Double-Blind, Placebo-Controlled, Global Phase III Trial of Talimogene Laherparepvec Combined With Pembrolizumab for Advanced Melanoma. *JCO* 2023;41:528–40.
5 Wong MK, Milhem MM, Sacco JJ, *et al*. RP1 Combined With Nivolumab in Advanced Anti–PD-1–Failed Melanoma (IGNYTE). *J Clin Oncol* 2025;43:3589–99.
6 Thomas S, Kuncheria L, Roulstone V, *et al*. Development of a new fusion-enhanced oncolytic immunotherapy platform based on herpes simplex virus type 1. *J Immunother Cancer* 2019;7:214.
7 Adair RA, Roulstone V, Scott KJ, *et al*. Cell carriage, delivery, and selective replication of an oncolytic virus in tumor in patients. *Sci Transl Med* 2012;4:138ra77.
8 Jiang Y, Chen M, Nie H, *et al*. PD-1 and PD-L1 in cancer immunotherapy: clinical implications and future considerations. *Hum Vaccin Immunother* 2019;15:1111–22.
9 Lei Q, Wang D, Sun K, *et al*. Resistance Mechanisms of Anti-PD1/PDL1 Therapy in Solid Tumors. *Front Cell Dev Biol* 2020;8:672.
10 Schönrich G, Raftery MJ. The PD-1/PD-L1 Axis and Virus Infections: A Delicate Balance. *Front Cell Infect Microbiol* 2019;9:207.
11 Hwang JK, Hong J, Yun CO. Oncolytic Viruses and Immune Checkpoint Inhibitors: Preclinical Developments to Clinical Trials. *IJMS* 2020;21:8627.
12 Devasthanam AS. Mechanisms underlying the inhibition of interferon signaling by viruses. *Virulence* 2014;5:270–7.

13 Coffelt SB, Wellenstein MD, de Visser KE. Neutrophils in cancer: neutral no more. *Nat Rev Cancer* 2016;16:431–46.
14 Xiong S, Dong L, Cheng L. Neutrophils in cancer carcinogenesis and metastasis. *J Hematol Oncol* 2021;14:173.
15 Mayadas TN, Cullere X, Lowell CA. The Multifaceted Functions of Neutrophils. *Annu Rev Pathol Mech Dis* 2014;9:181–218.
16 Huang X, Nepovimova E, Adam V, *et al*. Neutrophils in Cancer immunotherapy: friends or foes? *Mol Cancer* 2024;23:107.
17 Bert S, Nadkarni S, Perretti M. Neutrophil-T cell crosstalk and the control of the host inflammatory response. *Immunol Rev* 2023;314:36–49.